FINAL REPORT

to

National Fluid Power Association
Cooperative Network for Research in Motion Control through Fluid Power
(CNR)

NUMERICAL MODEL OF A RECIPROCATING ROD SEAL, INCLUDING SURFACE ROUGHNESS AND MIXED LUBRICATION

Richard F. Salant, Bo Yang and Nick Maser
George W. Woodruff School of Mechanical Engineering
Georgia Institute of Technology
Atlanta, Georgia 30332-0405

Project 2506-6KG

February 28, 2007

TABLE OF CONTENTS

I. SUMMARY

The objective of this project has been the development of a numerical model (and associated computer program) of a generalized reciprocating hydraulic rod seal, including mixed lubrication and surface roughness. This objective has been achieved. The resulting model predicts the key seal performance characteristics, such as leakage and friction. It is an elastohydrodynamic model and consists of coupled fluid mechanics, contact mechanics and deformation analyses. The model is in two forms: one for a single lip seal and the other for a double lip seal. In the latter case, mass conservation and the pressure of the intervening fluid couples the two lips to each other.

The leakage, film thickness distribution, fluid and contact pressure distributions and shear stress distributions have been predicted for both outstroke and instroke for a single lip seal and a double lip seal. The results show that, in general, hydraulic rod seals operate in the mixed lubrication regime, although under certain conditions full film lubrication may occur over a portion of the sealing zone. The roughness of the seal surface and the rod speeds play important roles in determining whether or not a seal will leak. Cavitation during the outstroke and partial full film lubrication during the instroke tend to prevent net leakage. The behavior of a seal with a double lip can be very different from that of a seal with a single lip, since the secondary lip can strongly affect the behavior of the primary lip by producing an elevated pressure in the interlip region. However, the same seal characteristics that promote effective sealing in a single lip seal are also found to promote effective sealing in a double lip seal: cavitation of fluid in the sealing zone during the outstroke and a thicker film during instroke than during outstroke.

II. INTRODUCTION

A serious potential problem in hydraulic systems is leakage of hydraulic fluid from the cylinders past the reciprocating rod seals. Not only can this leakage affect the system performance but, more importantly, it can lead to environmental pollution since such leakage directly enters the natural surroundings. Thus, the rod seal is the most critical of all hydraulic seals.

Research on reciprocating seals dates back to at least 1964 [1], [2]. Although much has been learned about the behavior of such seals, especially from experimental studies, their basic behavior is still poorly understood. This is primarily due to the absence of realistic theoretical models of seal operation. Consequently, the seal designer has virtually no analytical tools, beyond finite element structural analysis [3]-[6], with which to predict the behavior of potential seal designs or interpret test results. Neither does he/she have a conceptual framework upon which to base a design. Thus, current seal design is almost completely an empirical process.

A sketch of a typical hydraulic rod seal is shown in Figure 1. The region where the elastomeric seal lip appears to meet the rod is termed the sealing zone; it is where the sealing action takes place. Figure 2 shows how the sealing zone has been represented by most previous models: the surfaces of the rod and seal are assumed perfectly smooth and completely separated by a continuous film of hydraulic fluid, i.e. full film lubrication.

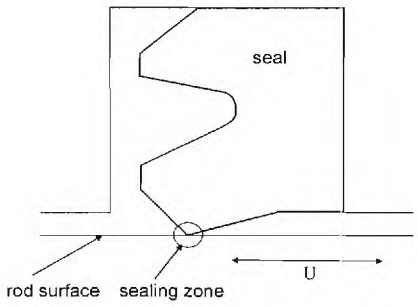

Figure 1: Typical hydraulic rod seal.

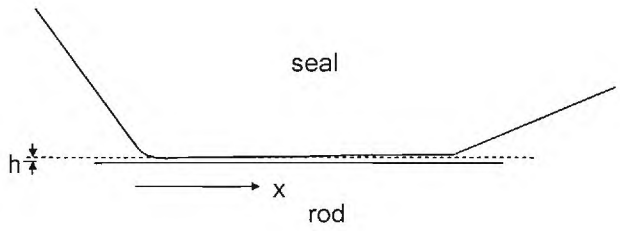

Figure 2: Sealing zone, as represented in previous models.

The analysis of the seal behavior is a problem in soft elastohydrodynamics, since the fluid pressure distribution in the sealing zone deforms the seal and affects the film

thickness distribution, while the film thickness distribution affects the fluid mechanics and determines the fluid pressure distribution. Previous models use one of two approaches: the direct method or the inverse method. In the direct method [7]-[10], the coupling between the fluid mechanics (governed by the Reynolds equation) and the deformation mechanics (governed by the elasticity equations) is handled through the use of iteration, leading to solutions for both the fluid pressure and film thickness distributions. In the inverse method [11]-[13], the fluid pressure distribution is assumed to equal the static contact pressure distribution, which is obtained from a deformation analysis. The Reynolds equation is then solved to yield the film thickness distribution.

Unfortunately, the neglect of roughness and the assumption of full film lubrication have been shown through experiment to be unrealistic [14]-[16], and have led to erroneous predictions. For example, studies using the inverse method predict that a seal which produces a static contact pressure distribution with a steep slope near the liquid side of the sealing zone and a gradual slope near the air side, will not leak provided the ratio of the outstroke rod speed to the contact pressure slope on the liquid side is less than the ratio of the instroke rod speed to the contact pressure slope on the air side [11]. Experience has shown that this is not necessarily true.

In the present study, the assumptions of zero roughness and full film lubrication have been eliminated. It should be noted that a recent series of papers also takes account of surface roughness and mixed lubrication, but is limited to a special class of seals, those with a rectangular cross-section [17]-[19].

III. ANALYSIS – SINGLE LIP SEAL

Figure 3 shows the sealing zone, as it is represented in the present model, in a state of mixed lubrication. The seal surface is considered rough, while the rod surface is treated as smooth. Note that although the sketch shows the film thickness as constant, it is a function of axial location, x. The fluid mechanics of the lubricating film is governed by Reynolds equation. Since cavitation is possible in portions of the film, a form of Reynolds equation that accounts for such cavitation is required.

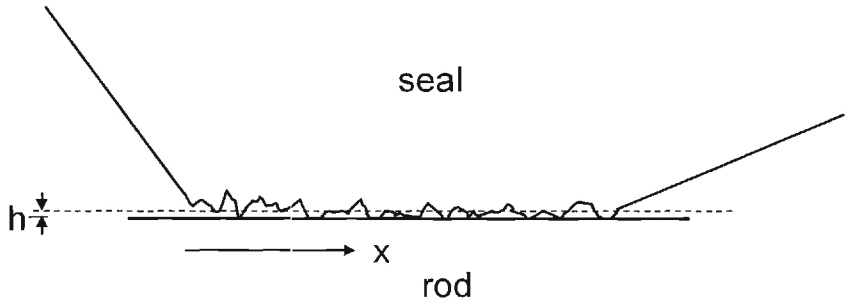

Figure 3: Sealing zone, as represented in present model.

In dimensionless terms,

$$\frac{d}{d\hat{x}}\left[\phi_{xx}H^3 e^{-\hat{\alpha}F\phi}\frac{dF\phi}{d\hat{x}}\right] = 6\zeta\left[\frac{d}{d\hat{x}}\left\{\left[1+(1-F)\phi\right]H_T\right\} + F\frac{d\phi_{s.c.x}}{d\hat{x}}\right] \quad (1)$$

F is the cavitation index, while ϕ is equal to the pressure in the liquid region and is related to the average density in the cavitated region. Thus, in the liquid region,

$$\phi \geq 0 \quad F = 1 \text{ and } P = \phi \quad (2)$$

while in the cavitated region,

$$\phi < 0 \quad F = 0 \text{ and } P = 0, \hat{\rho} = 1 + \phi \quad (3)$$

The boundary conditions are,

$$\begin{aligned} \phi &= P_{sealed} \quad at\ \hat{x} = 0 \\ &= 1 \qquad at\ \hat{x} = 1 \end{aligned} \quad (4)$$

The average truncated film thickness is given by,

$$H_T = \int_{-H}^{\infty} [H + \delta] f(\delta) d\delta \tag{5}$$

which, for a Gaussian distribution is,

$$H_T = \frac{H}{2} + \frac{H}{2} erf\left(\frac{H}{\sqrt{2}}\right) + \frac{1}{\sqrt{2\pi}} e^{\left(\frac{-H^2}{2}\right)} \tag{6}$$

ϕ_{xx} and $\phi_{s.c.x}$ are flow factors that take into account the effect of the surface roughness of the seal lip. They are functions of the ratio of the film thickness to the roughness amplitude and the roughness geometry (aspect ratio and orientation of the asperities), and are obtained from [20], [21].

The Reynolds equation, eq. (1), is put into finite difference form and solved for ϕ and F for given values of H, using the tri-diagonal matrix algorithm. This yields the pressure distribution and the locations of cavitating regions. The flow rate (per unit circumferential length) and the shear stress on the rod can then be computed from,

$$\hat{q} = -\phi_{xx} e^{-\hat{\alpha} F \phi} H^3 \frac{dF\phi}{dx} + 6\zeta \left\{ \left[1 + (1 - F)\phi \right] H_T + F\phi_{s.c.x} \right\} \tag{7}$$

and,

$$\hat{\tau}_{avg} = \frac{\tau_{avg}}{E} = \frac{-\hat{\sigma}}{\xi} e^{-\hat{\alpha} F \phi} \frac{\zeta}{H} \left(\phi_f - \phi_{fss} \right) - \phi_{fpp} \frac{\hat{\sigma}}{\xi} \frac{H}{2} \frac{dF\phi}{d\hat{x}} \tag{8}$$

The shear stress flow factors, ϕ_f , ϕ_{fss}, and ϕ_{fpp} are obtained from [21].

The contact mechanics analysis is based on the Greenwood and Williamson surface contact model [22]. Assuming a Gaussian distribution of asperities, the contact pressure is computed from,

$$P_c = \frac{4}{3}\frac{1}{\left(1-\nu^2\right)}\hat{\sigma}^{\frac{3}{2}}\frac{1}{\sqrt{2\pi}}\int_H^{\infty}\left(z-H\right)^{\frac{3}{2}}e^{-\frac{z^2}{2}}dz \tag{9}$$

and the frictional shear stress on the rod, from,

$$\hat{\tau}_c = -fP_c\left(\frac{\varsigma}{|\varsigma|}\right) \tag{10}$$

using a friction coefficient, f.

To compute the film thickness distribution, it is necessary to compute the radial (normal) deformation of the sealing element. This is done within an iteration loop, so it is necessary to use a computationally efficient method. The influence coefficient method has been chosen. With this method it is recognized that the deformation at any location is proportional to the forces applied at every location. Thus, in discretized form with n axial nodes across the sealing zone, the film thickness at the ith node can be expressed as,

$$H_i = H_s + \sum_{k=1}^{n}(I_1)_{ik}(P_t - P_{sc})_k \tag{11}$$

so the on-line model contains only linear algebraic equations. The proportionality factors $(I_1)_{ik}$ the "influence coefficients," are computed off-line using a commercial finite element analysis code. The pressure P_t is the sum of the fluid and contact pressures. P_{sc} is the static contact pressure distribution, computed off-line with the same finite element code used to obtain the influence coefficients.

The static film thickness, H_s, is computed by equating the static contact pressure obtained from the finite element analysis, P_{sc}, with the contact pressure distribution computed from eq. (9) under static conditions. Using the approximate method of [23] to invert eq. (9) yields,

$$H_s = -1.0641 + \left(3.6305 - 5.0684\log_{10} I\right)^{1/2} \tag{12}$$

where,

$$I = \frac{P_{sc}}{\frac{4}{3}\frac{1}{\left(1-\nu^2\right)}\hat{\sigma}^{\frac{3}{2}}} \tag{13}$$

Since the above equations are all strongly coupled, an iterative computation procedure, shown in Figure 4, is required.

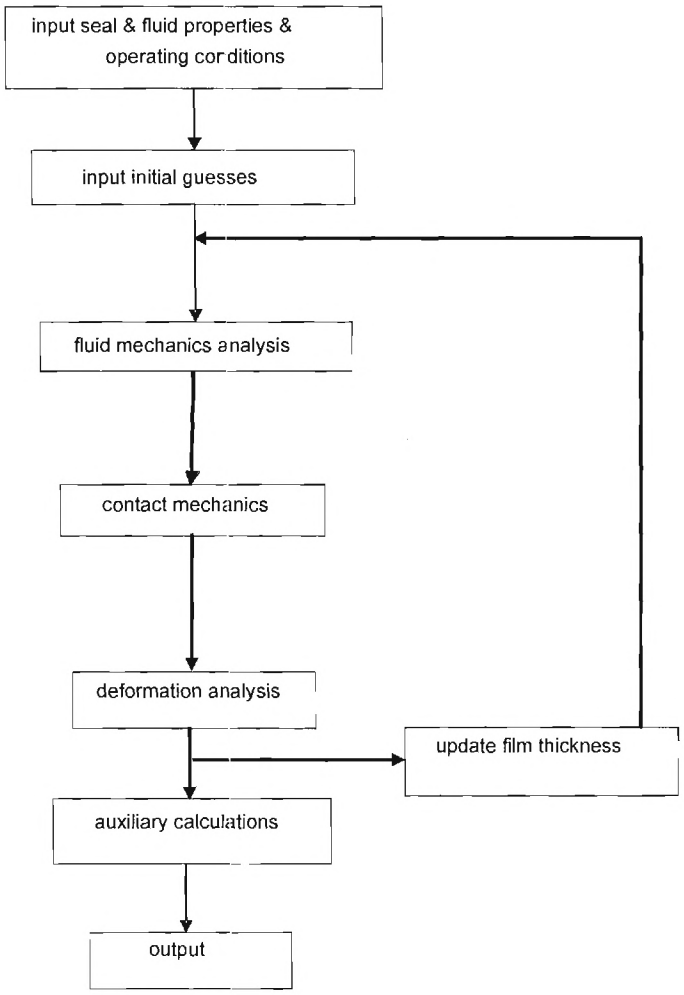

Figure 4: Computational procedure.

Following input of the seal properties, fluid properties and operating conditions, initial guesses of the film thickness (uniform) and cavitation index (1, everywhere) are input. The fluid mechanics analysis is then performed to yield the fluid pressure distribution. An inner iteration loop (not shown in figure) is required because the viscosity is pressure dependent and because the cavitation index must be updated. Next, the contact mechanics analysis is performed to yield the contact pressure distribution, and the deformation

analysis is performed to yield the normal deformations. The film thickness distribution is then updated, and iteration continues until the solution converges. Auxiliary calculations yield the flow rate and frictional shear stress. A one-dimensional mesh with 196 nodes is used (selected following a mesh sensitivity study).

It should be noted that for a given dimensionless static contact pressure distribution and dimensionless influence coefficients, the dimensionless film thickness, fluid pressure and contact pressure distributions, and the dimensionless flow rate, are functions of the dimensionless rod speed ζ and the dimensionless roughness $\hat{\sigma}$. The dimensionless total shear stress $[\hat{\tau}_{avg}]_t$ is, in addition, dependent on ξ.

IV. RESULTS – SINGLE LIP SEAL

Computations have been performed for a typical hydraulic rod seal, with base parameters shown in Table 1.

Figure 5 shows the film thickness distribution for the outstroke and the instroke. Since significant asperity contact occurs when the film thickness is less than 3σ (for the base seal, less than 0.9 μm), it is clear that during the outstroke the entire sealing zone experiences mixed lubrication. During the instroke, mixed lubrication also occurs near the liquid side of the sealing zone, although full film lubrication occurs over a substantial area near the air side. Thus it is clear that the assumption of full film lubrication in previous models is not justified.

The pressure distributions in the sealing zone for the outstroke are shown in Figure 6. As can be seen, the contact pressure distribution has a steep slope near the liquid side of the zone and a more gradual slope near the air side. For such a profile, the full film theory models predict no leakage [11], as mentioned earlier.

		dimensionless
Elastic modulus	43 x 10^6 Pa	
Poisson's ratio	0.49	
Sealed pressure	6.90 MPa (1000 psi)	
Rod diameter	88.9 mm (3.5")	
Stroke	1.93 m (76")	
Speed - outstroke	0.635 m/s (25 in/s)	973
Speed - instroke	-0.813 m/s (-32 in/s)	-1245
Reference viscosity	0.043 Pa-s	
Pressure-viscosity coefficient	20 x 10^{-9} Pa^{-1}	20 x 10^{-4}
Asperity radius	1 μm	6.401 x 10^4
RMS roughness	0.3 μm	1.392
Asperity density	10^{13} m^{-2}	
Sealing zone length	0.321 mm	
Asperity contact friction coefficient	0.25	

Table 1: Base seal parameters.

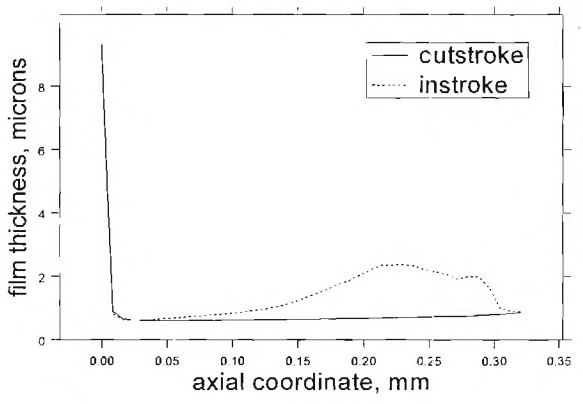

Figure 5: Film thickness distributions, base case.

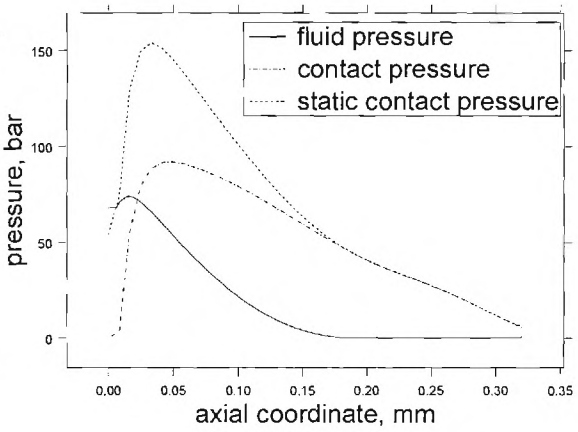

Figure 6: Pressure distributions – outstroke, base case.

Hydrodynamic pressure generation causes the fluid pressure to be elevated near the liquid side of the zone, slightly lifting the seal away from the rod. This reduces the contact pressure below its static value in that region. However, over almost half of the

sealing zone, near the air side, the fluid is cavitated (zero pressure), and therefore the contact pressure equals its static value.

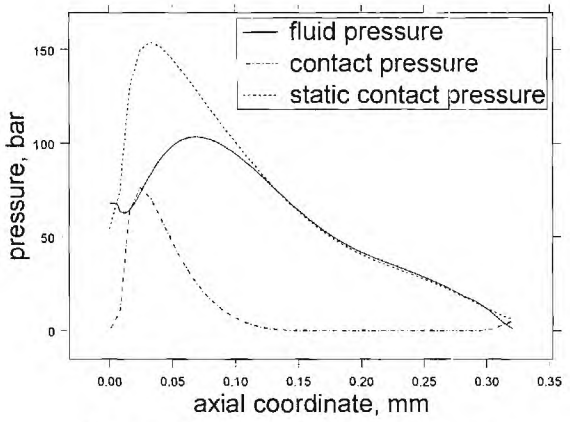

Figure 7: Pressure distributions – instroke, base case.

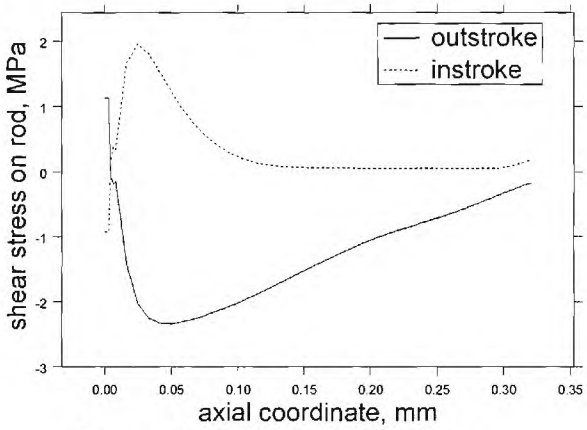

Figure 8: Frictional shear stress distributions, base case.

Figure 7 shows the pressure distributions for the instroke. There is significantly more hydrodynamic pressure generation than during the instroke, which causes the lip to lift completely off the rod near the air side, resulting in full film lubrication over more than half of the sealing zone. In this region the contact pressure is zero. This effect was also seen in Figure 5.

The frictional shear stress on the rod is shown in Figure 8. As would be expected, it is in opposite directions for the instroke and the outstroke. The peak stresses are near the liquid side of the sealing zone, where the contact pressures are highest. The corresponding friction coefficients are 0.192 for the outstroke and 0.051 for the instroke. The volume of fluid carried out during the outstroke, for this base seal, is computed as 0.237 cc/stroke, while the volume the seal is capable of drawing back in during the instroke, is computed as 0.249 cc/stroke. Since the latter exceeds the former, there is no net leakage during a cycle, and one could say that this seal does not leak.

The base case seal has an rms roughness of 0.3 μm. Figure 9 shows how the seal roughness affects the leakage characteristics. It is a plot of the fluid transport (volume of fluid carried out during the outstroke or volume of fluid capable of being drawn in during the instroke) versus rms roughness. All parameters other than the seal roughness are equal to the base values. Note that for a seal to be non-leaking the fluid transport for the outstroke must be larger than that for the instroke. The base case is denoted on the plot by

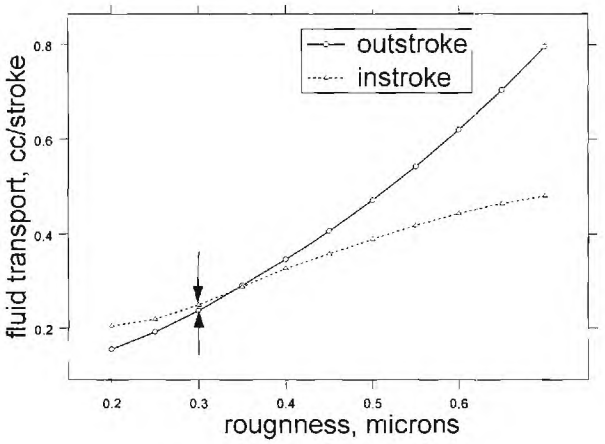

Figure 9: Fluid transport vs. roughness.

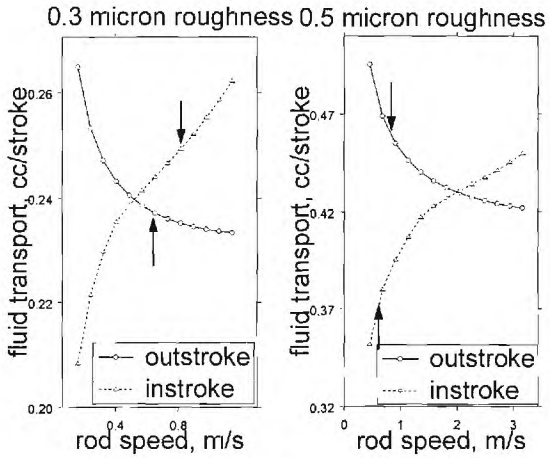

Figure 10: Fluid transport vs. rod speed.

the arrows. As stated, above, the base case is non-leaking. From the plot it is seen that there is no net leakage for roughness values less than 0.35 μm. However, for higher values of roughness, larger than 0.35 μm, the seal would leak. The larger than roughness, the larger would be the leakage. This directly contradicts the results of previous full film models, which would predict zero leakage for this seal, regardless of the roughness.

Figure 10 is a plot of fluid transport vs. rod speed for the base case seal with 0.3 μm roughness and for a similar seal with 0.5 μm roughness. This type of plot would be very useful when designing or selecting a seal, since it shows the combinations of roughness and rod speeds which would result in a non-leaking seal. The arrows denote the seal operating points at the base rod speeds. As seen on this plot, as well as on the plot in Figure 9, the 0.3 μm roughness seal is non-leaking while the 0.5 μm roughness seal leaks. To eliminate leakage from the latter seal, the rod speeds would have to be raised considerably, to values above 2 m/s.

It is instructive to compare these two seals, the 0.3 μm and 0.5 μm roughness seals, both with the same rod speeds, one non-leaking and one leaking. The fluid transports for the various strokes are shown in Table 2. Note that increasing the roughness to 0.5 μm, increases the volume of fluid carried out during the outstroke relative to that carried in during the instroke, such that the former exceeds the latter, leading to net leakage. The causes of this change can be seen by examining the pressure

and film thickness distributions for the 0.5 μm roughness seal, Figures 11-13, and comparing them with the corresponding distributions for the 0.3 μm roughness seal.

	0.5 μm roughness seal leaking	0.3 μm roughness seal non-leaking
fluid transport - outstroke	0.473 cc/stroke	0.237 cc/stroke
fluid transport - instroke	0.390 cc/stroke	0.249 cc/stroke

Table 2: Comparison between leaking & non-leaking seals.

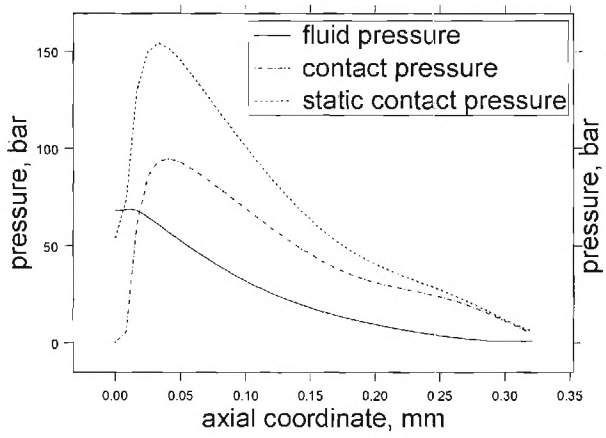

Figure 11: Pressure distributions – outstroke, 0.5 μm roughness.

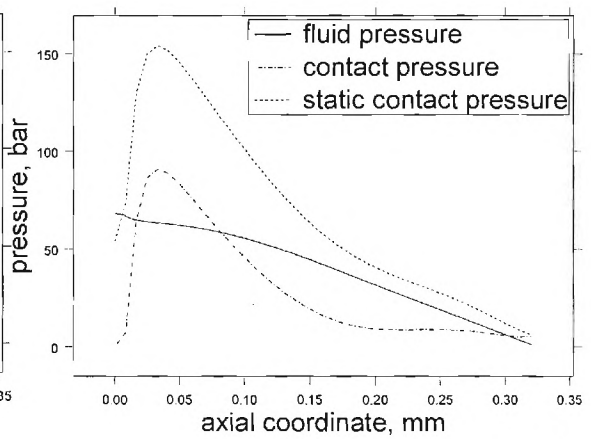

Figure 12: Pressure distributions – instroke, 0.5 μm roughness.

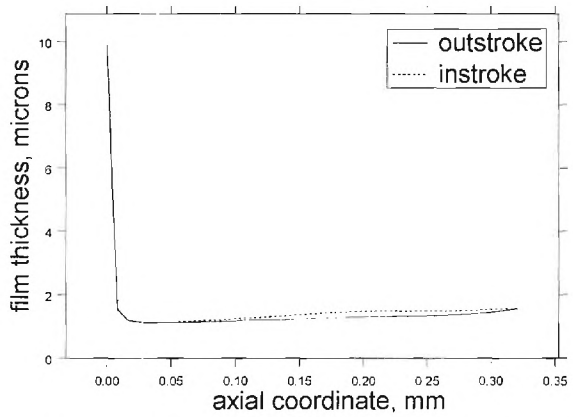

Figure 13: Film thickness distributions, 0.5 μm roughness.

Comparison of Figures 11 and 6 shows that the cavitation that occurs during the outstroke in the non-leaking 0.3 μm roughness seal is eliminated from the leaking 0.5 μm roughness seal. This cavitation reduces the volume of fluid that is carried out of the cylinder. Comparison of Figures 12 and 6, and Figures 13 and 5 shows that the full film lubrication over a portion of the sealing zone during the instroke of the 0.3 μm roughness seal is eliminated from the 0.5 μm roughness seal, whose entire sealing zone experiences mixed lubrication. Full film lubrication increases the volume of fluid that can be drawn back into the cylinder.

V. ANALYSIS – DOUBLE LIP SEAL

While many seals have a single lip, there are some seals which have two lips. The secondary lip is intended to act as a second line of defense, as well as a bearing. It is important to understand the behavior of such a double lip seal, and how that behavior differs from that of a single lip seal.

Figure 14 contains a schematic of a typical reciprocating rod seal with a double lip.

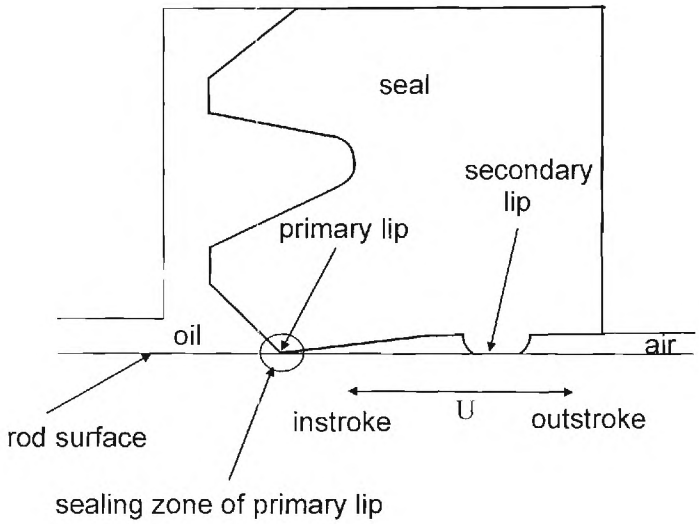

Figure 14: Double lip seal.

In Section IV a seal with only the primary lip is analyzed using a model consisting of a fluid mechanics analysis, a contact mechanics analysis, a deformation

analysis and an iterative computational procedure. In the present section a similar approach is applied to each lip.

There are two primary differences between the analyses of the double lip and single lip cases, which complicate the double lip model. First, under steady state conditions (which are assumed), the mass flow rate past the two lips must be the same for the double lip seal, a restriction absent for the single lip seal. Second, the boundary conditions on the fluid in the sealing zone are different. For the single lip seal, the fluid pressure at the inner boundary (liquid side) is equal to the sealed pressure while that at the outer boundary (air side) is equal to the ambient pressure. These pressures are known a priori. For the double lip seal, boundary conditions must be applied to both lips. For the primary lip, the fluid pressure at the inner boundary is again equal to the sealed pressure, but that at the outer boundary is equal to the pressure in the interlip region (see Figure 14), provided the fluid is not cavitated. For the secondary lip, the fluid pressure at the inner boundary is also equal to the pressure in the interlip region, provided the fluid is not cavitated, while that at the outer boundary is equal to the ambient pressure. If the fluid in and near the interlip region is cavitated, then the average fluid density at the outer boundary of the primary lip must be equal to that at the inner boundary of the secondary lip. It should be noted that the conditions in the interlip region are not known a priori, and must be determined in the course of the analysis. From these considerations it is clear that the behavior of the two lips in a double lip seal are coupled.

As discussed above, the boundary conditions on the Reynolds Equation, eq. (4), for the single lip seal is replaced by eq. (14) for the primary and secondary lips of the double lip seal.

$$\begin{aligned} \phi_{primary} &= P_{sealed} \quad at\ \hat{x} = 0 \\ &= \phi_{interlip} \quad at\ \hat{x} = 1 \end{aligned}$$

$$\begin{aligned} \phi_{secondary} &= \phi_{interlip} \quad at\ \hat{x} = 0 \\ &= 1 \qquad\quad at\ \hat{x} = 1 \end{aligned} \tag{14}$$

Also as discussed above, the mass the flow rates through the sealing zones of the two lips must be equal.

$$\hat{q}_{primary} = \hat{q}_{secondary} \tag{15}$$

It should be noted that the two lips are also coupled through the deformation characteristics of the seal. Similar to the analysis of the single lip seal, the influence coefficients and static contact pressure distribution for each lip is obtained from a finite element structural analysis. One of the boundary conditions in that analysis involves the fluid pressure/density in the interlip region, which is jointly determined by the action of both lips.

This last form of coupling requires special treatment since the finite element analysis is done off-line and the interlip pressure/density is not known a priori. A series of finite element analyses are therefore performed for a number of specified discrete interlip pressures spanning the expected range. Depending on the computed interlip pressure/density, the appropriate finite element solution for the static contact pressure distribution and the influence coefficients is used in the iterative computation procedure, shown below.

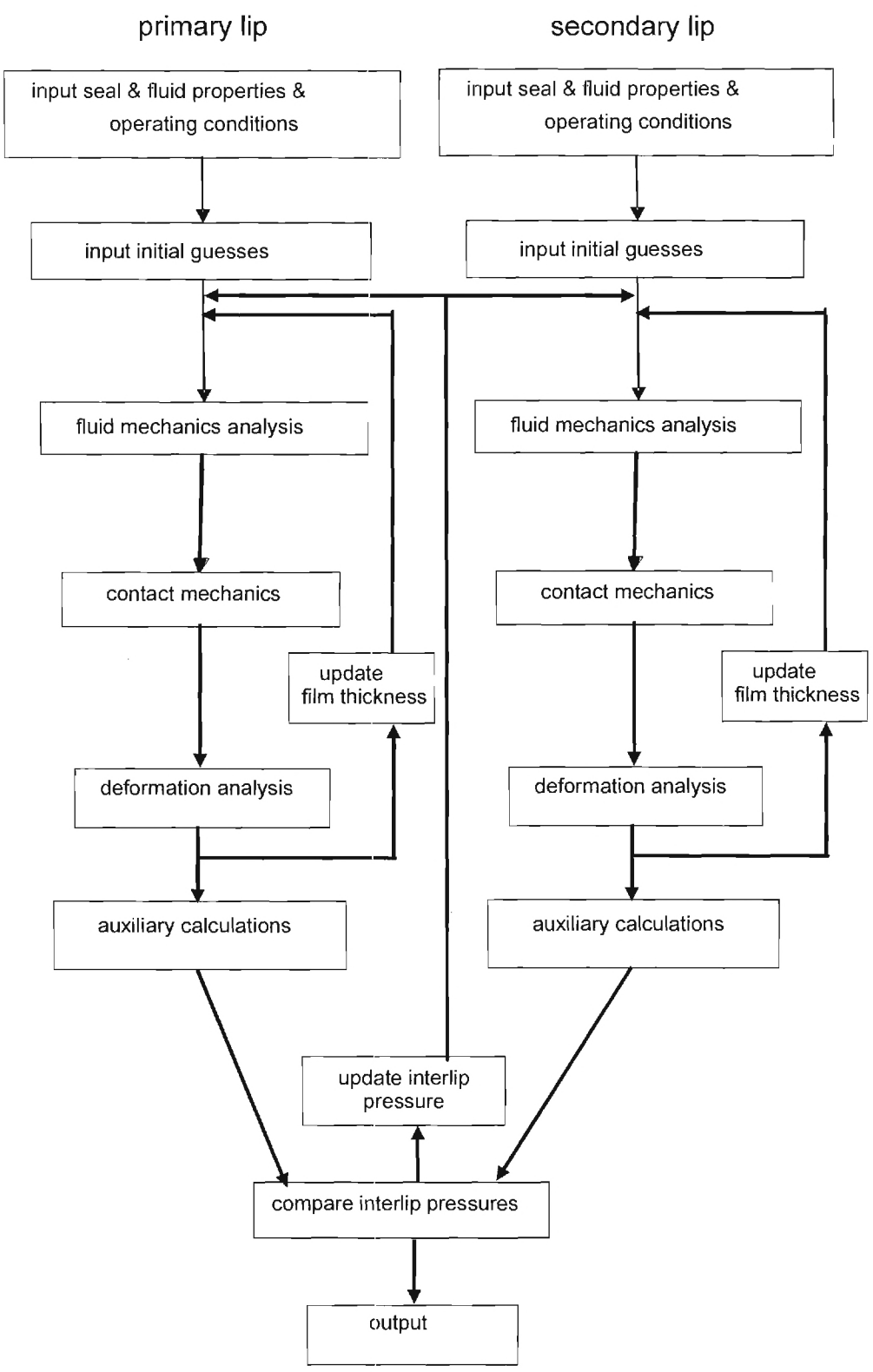

Figure 15: Computational procedure.

VI. RESULTS – DOUBLE LIP SEAL

Computations have been performed for a typical seal with base parameters of : E = 43 x 10^6 Pa, υ = 0.49, p_{sealed} = 6.90 MPa (1000 psi), U = 0.635 m/s (25 in/s) outstroke, U = -0.813 m/s (-32 in/s) instroke, μ_0 = 0.043 Pa-s, α = 20 x 10^{-9} Pa^{-1}, R = 1.0 μm, η = 10^{13} m^{-2}, f = 0.25, rod diameter = 88.9 mm (3.5 in). The roughness is assumed to be isotropic.

The presence of the secondary lip can significantly change the geometry of the primary lip due to its effect on the pressure in the interlip region (discussed below). For example with a roughness of 0.6 μm, the length of the primary lip sealing zone is approximately 0.3 mm during an outstroke while it is approximately 1.4 mm during an instroke. Thus, while with a single lip seal there is no significant difference in the sealing zone length for an outstroke and an instroke, with a double lip seal, there are such differences for both the primary and secondary lips.

The interlip pressure is shown as a function of roughness in Fig. 16. For the outstroke, as the roughness is decreased from a value of σ = 1.4 μm, the interlip pressure increases until it reaches a maximum of 88 bar (compared to the sealed pressure of 69 bar) at a roughness of σ = 0.4 μm, whereupon it decreases rapidly with a further reduction in roughness. Conversely, for the instroke the interlip pressure decreases with decreasing roughness until a roughness of σ = 0.8 μm, at and below which the fluid in the interlip region cavitates.

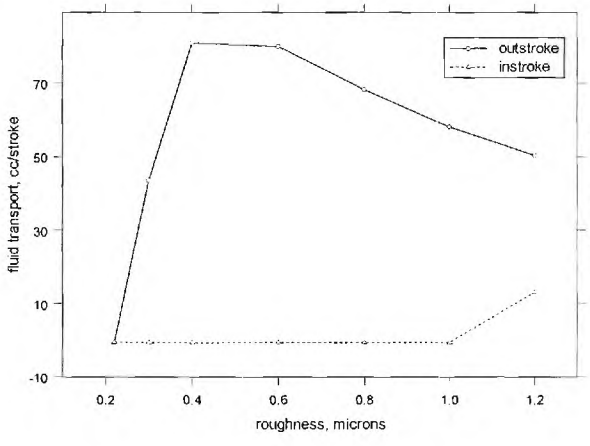

Figure 16: Interlip pressure vs. roughness

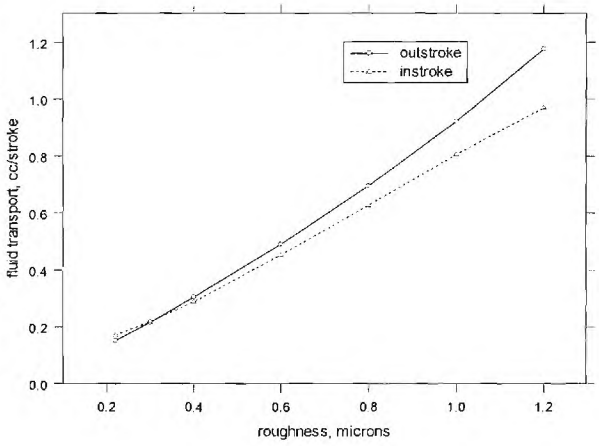

Figure 17: Fluid transport vs. roughness.

Figure 17 contains a plot of the fluid transport during instroke and outstroke for the double lip seal. As discussed earlier, for zero net leakage, the instroke fluid transport must exceed the outstroke transport. This occurs at values of roughness below a critical roughness of approximately 0.3 μm.

Figures 18-23 describe the behavior of the double lip seal with a roughness of 0.22 μm, a non-leaking seal under the base conditions. The film thickness distributions of the primary lip, Fig. 18, show that the lip operates with mixed lubrication since the thicknesses are always less than 3σ. It should also be noted that the film thickness during the instroke exceeds that during an outstroke, which is a characteristic that promotes non-leakage [24-26]. However the lengths of the sealing zone during outstroke and instroke are the same. This is not surprising, since Fig. 16 indicates the pressure in the interlip region is the virtually the same for both strokes.

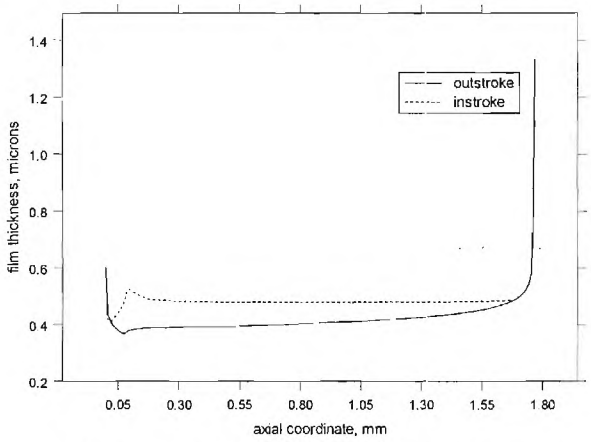

Figure 18: Film thickness distributions, primary lip, 0.22 μm roughness.

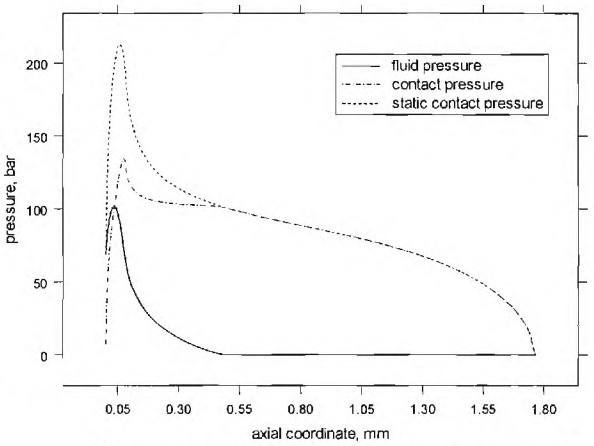

Figure 19: Pressure distributions – primary lip, outstroke, 0.22 μm roughness.

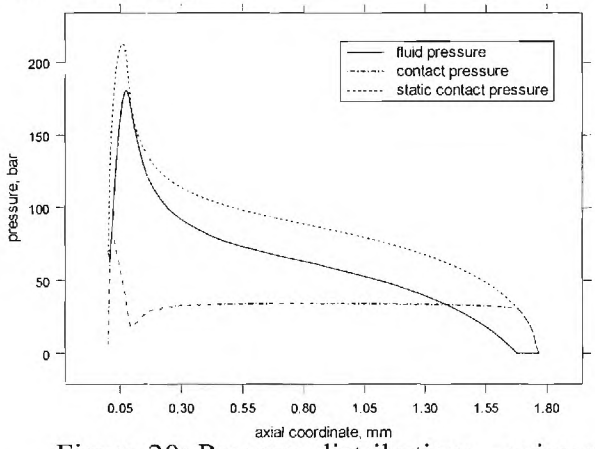

Figure 20: Pressure distributions – primary lip, instroke, 0.22 μm roughness.

The fluid pressure, contact pressure and static contact pressure distributions of the primary lip for the outstroke are shown in Fig. 18. From the fluid pressure distribution it is clear that the fluid cavitates over most of the sealing zone, again a characteristic that promotes non-leakage since the cavitation restricts the outflow of fluid. The corresponding figure for the instroke, Fig. 19, shows only a very small portion of the sealing zone cavitating. This, too, promotes non-leakage since the lack of cavitation during the instroke allows greater transport of fluid inward. These primary lip characteristics are very similar to those of a comparable single lip seal in a non-leaking condition [24-26].

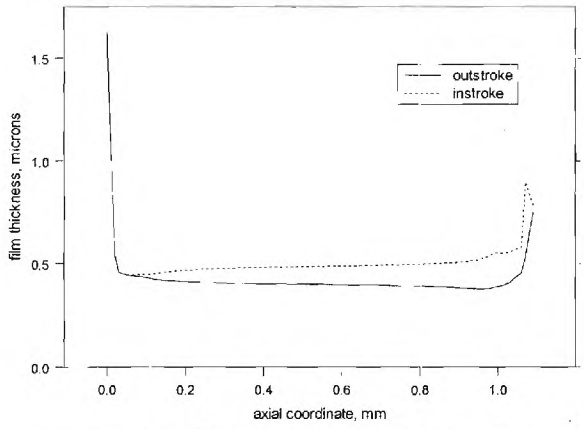

Figure 21: Film thickness distributions, secondary lip, 0.22 μm roughness.

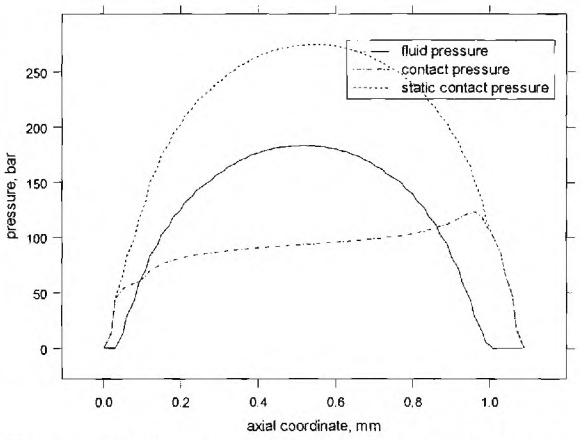

Figure 22: Pressure distributions – secondary lip, outstroke, 0.22 μm roughness.

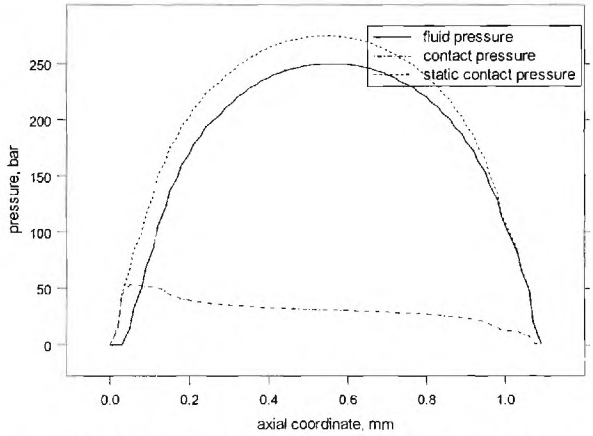

Figure 23: Pressure distributions – secondary lip, instroke, 0.22 μm roughness.

The film thickness and pressure distributions of the secondary lip are shown in Figs. 21-23. These, similarly, indicate mixed lubrication, and have characteristics that promote non-leakage: the film thickness during instroke is larger than that during

outstroke; there is some cavitation during the outstroke to restrict outflow and no cavitation during the instroke allowing greater transport of fluid inward. The pressure distributions of the secondary lip are much more symmetric than those of the primary lip due to the secondary lip's symmetric shape.

It is useful to compare the above results for a non-leaking seal with those for a leaking seal: the same double lip seal but with a surface roughness of 0.6 μm, which Fig. 6 indicates will leak. The behavior of such a seal is shown in Figs. 24-29.

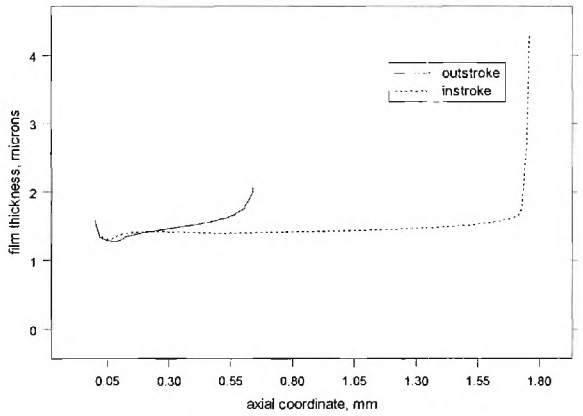

Figure 24: Film thickness distributions, primary lip, 0.6 μm roughness.

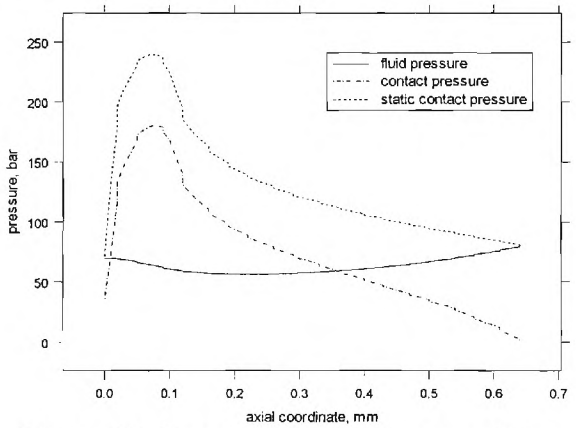

Figure 25: Pressure distributions – primary lip, outstroke, 0.6 μm roughness.

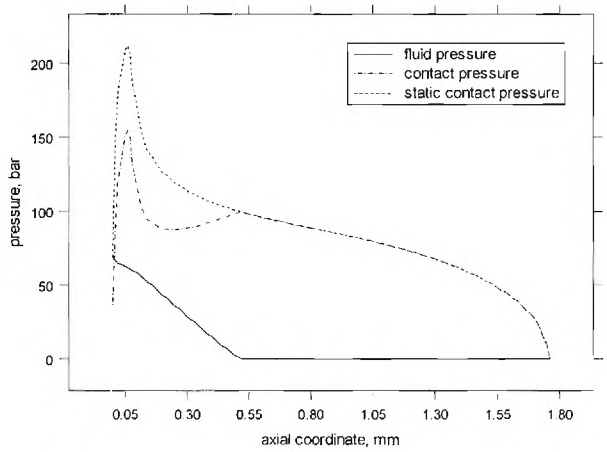

Figure 26: Pressure distributions – primary lip, instroke, 0.6 μm roughness.

The film thickness distributions of the primary lip, Fig. 24, again indicate mixed lubrication. Here, however, we see the length of the sealing zone is much shorter during the outstroke than during the instroke, as mentioned earlier. Also, at proportional

locations along the length of the sealing zone, the film thicknesses are larger for the outstroke than for the instroke. Both of these characteristics are detrimental for effective sealing, compared to the corresponding characteristics of the previously described non-leaking seal.

Figures 25 and 26 show the pressure distributions of the primary lip. From these it is seen that there is no cavitation during the outstroke and a significant amount of cavitation during the instroke. This is the opposite of what occurs in the non-leaking seal where cavitation helped prevent leakage; here it promotes leakage and is therefore detrimental.

The same general behavior is exhibited by the secondary lip, Figs.27-29: mixed lubrication and the detrimental effect of cavitation (although there is a small amount of cavitation present during the outstroke).

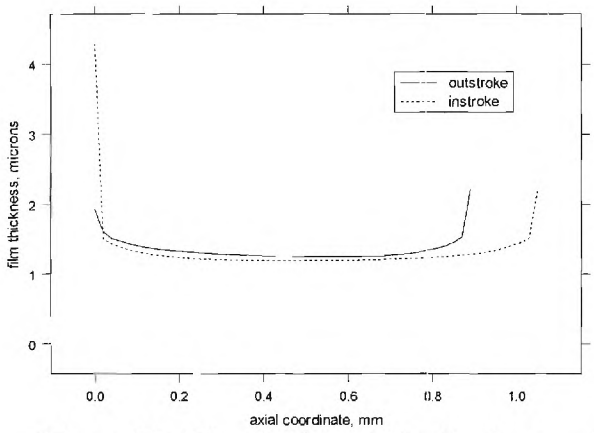

Figure 27: Film thickness distributions, secondary lip, 0.6 μm roughness.

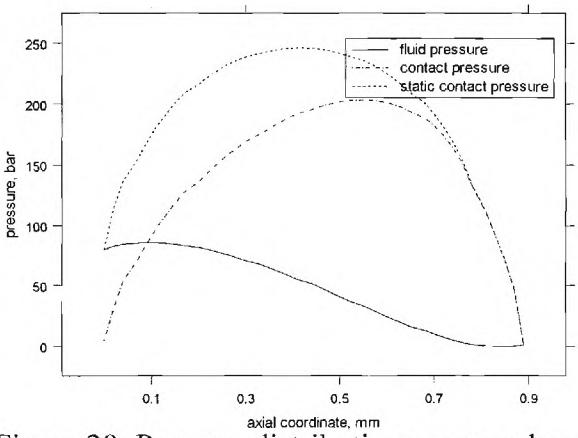

Figure 28: Pressure distributions – secondary lip, outstroke, 0.6 μm roughness.

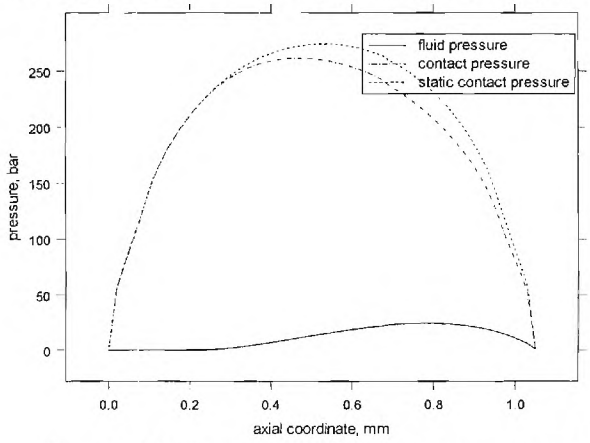

Figure 29: Pressure distributions – secondary lip, instroke, 0.22 μm roughness.

In addition to the film thickness and pressure distribution results for the double lip seal, shear stress distributions have also been generated. These are shown in Figs. 30 and 31 for the 0.22 μm case, and in Figs. 32 and 33 for the 0.6 μm case.

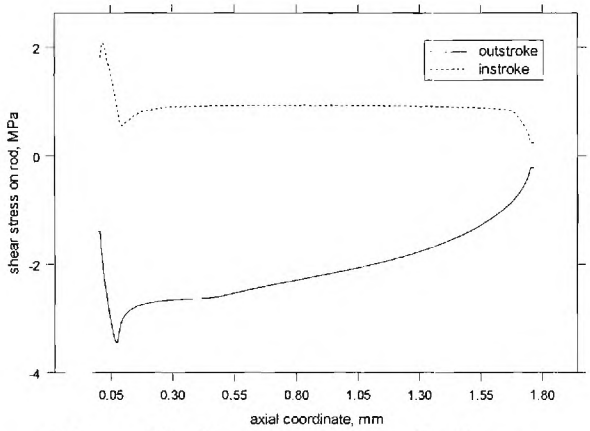

Figure 30: Shear stress distributions, primary lip, 0.22 μm roughness.

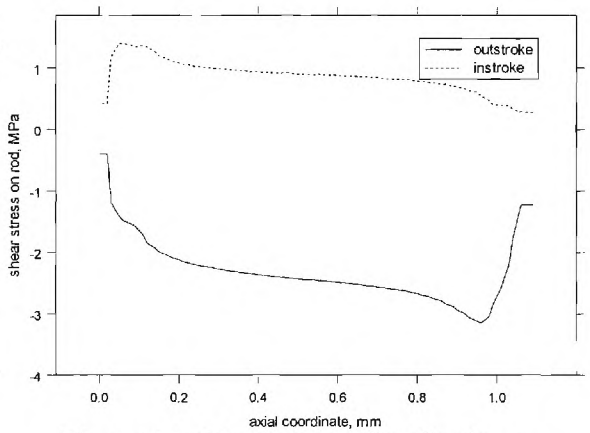

Figure 31: Shear stress distributions, secondary lip, 0.22 μm roughness.

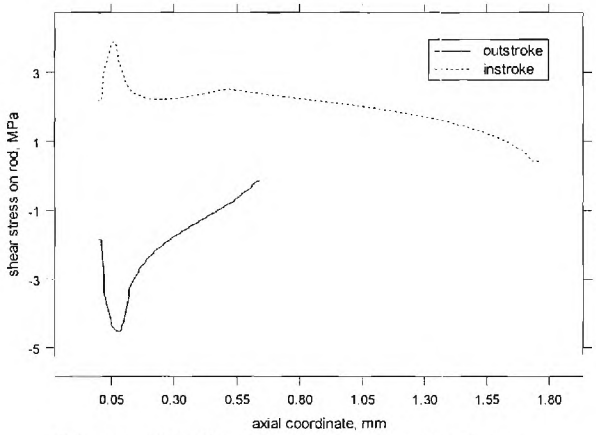

Figure 32: Shear stress distributions, primary lip, 0.6 μm roughness.

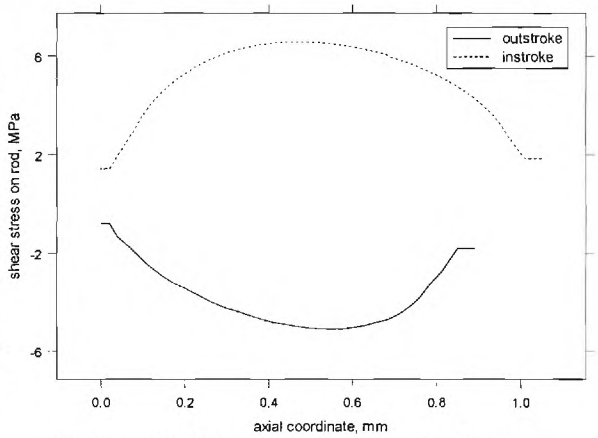

Figure 33: Shear stress distributions, secondary lip, 0.6 μm roughness.

VII. CONCLUSIONS

The results of this study show that, in general, hydraulic rod seals operate in the mixed lubrication regime, although under certain conditions full film lubrication may occur over a portion of the sealing zone. The roughness of the seal surface and the rod speeds play important roles in determining whether or not a seal will leak. Cavitation during the outstroke and partial full film lubrication during the instroke tend to prevent net leakage. The behavior of a reciprocating hydraulic rod seal with a double lip can be

very different from that of a seal with a single lip. The secondary lip can strongly affect the behavior of the primary lip by producing an elevated pressure in the interlip region. However, the same seal characteristics that promote effective sealing in a single lip seal are also found to promote effective sealing in a double lip seal: cavitation of fluid in the sealing zone during the outstroke and a thicker film during instroke than during outstroke.

VIII. NOMENCLATURE

E	elastic modulus
F	cavitation index
f	friction coefficient
$f(\delta)$	probability density function of roughness
H	dimensionless average film thickness, h/σ
H_s	static undeformed film thickness, h_s/σ
H_T	dimensionless average truncated film thickness, h_T/σ
I_l	influence coefficient for normal (radial) deformation
I	function defined by Eq. (12)
L	length of solution domain in x-direction
P	dimensionless fluid pressure, p/p_a
p_a	ambient pressure
P_c	dimensionless contact pressure for deformation analysis, p_c/E
P_{def}	dimensionless fluid pressure for deformation analysis, $P(p_a)/E$
P_{sc}	dimensionless static contact pressure, p_{sc}/E
P_{sealed}	dimensionless sealed pressured, p_{sealed}/p_a
P_t	dimensionless total pressure, $P_{def} + P_c$
$\hat{q}$	dimensionless flow rate per unit circumferential length, $12\mu_0 qL/[(p_a)\sigma^3]$
R	asperity radius
U	surface speed of rod
$\hat{x}$	dimensionless axial coordinate, x/L
$\hat{\alpha}$	dimensionless pressure-viscosity coefficient, αp_a
ϕ	fluid pressure/density function, defined by Eqs. (2) and (3)

$\phi_f, \phi_{fss}, \phi_{fpp}$	shear stress factors
$\phi_{s.c.x}$	shear flow factor
ϕ_{xx}	pressure flow factor
μ_0	viscosity at atmospheric pressure
$\hat{\rho}$	dimensionless density, ρ / ρ_l
ρ_l	liquid density
$\hat{\sigma}$	dimensionless rms roughness of sealing element surface, $\sigma R^{1/3} \eta^{2/3}$
$\hat{\tau}_{avg}$	average dimensionless viscous shear stress in the x-direction, τ_{avg}/E
$\hat{\tau}_c$	dimensionless shear stress due to contacting asperities, τ_c / E
$[\hat{\tau}_{avg}]_t$	total shear stress, $\hat{\tau}_{avg} + \hat{\tau}_c$
υ	Poisson's ratio
ξ	$R^{1/3} \eta^{2/3} EL / p_a$
ζ	dimensionless rod speed, $(\mu_0 UL)/[(p_a)\sigma^2]$
0	asperity density

IX. REFERENCES

1. Ishiwata, H. and Kambayashi, H., 1964, "A Study of Oil Seal for Reciprocating Motion," *Proc. 2nd BHRA International Conference on Fluid Sealing*, B3.
2. O'Donogue, J. P. and Lawrie, J. M., 1964, "The Mechanism of Lubrication in a Reciprocating Seal," *Proc. 2nd BHRA International Conference on Fluid Sealing*, B6.
3. Claus, R. G., 2002, "Development of a High Performance, Heavy Duty Piston Seal," *Proc. 49th National Conference on Fluid Power*, NFPA, pp. 383-389.
4. Peng, S., Sun, S. and Albertson, K., 1996, "FEA-Assisted Design of Low-Friction U-Cup as Spool Valve Seals," *Proc. 47th National Conference on Fluid Power*, NFPA, pp. 175-182.

5. Naderi, A., Albertson, K. and Peng, S., 1994, "Finite Element Analysis of a Hydraulic Seal: BS U-Cup," *Proc. 46th National Conference on Fluid Power*, NFPA, pp. 99-105.
6. Weiss, H., 1996, "New Generation of Hydraulic Seals Supports Progress for Hydraulic Cylinders," *Proc. 47th National Conference on Fluid Power*, NFPA, pp. 153-163.
7. Field, G. J. and Nau, B. S., 1974, "A Theoretical Study of the Elastohydrodynamic Lubrication of Reciprocating Rubber Seals," ASLE Transactions, **18**, pp. 48-54.
8. Ruskell, L. E. C., 1980, "A Rapidly Converging Theoretical Solution to the Elastohydrodynamic Problem for Rectangular Rubber Seals," J. Mechanical Engineering Science, **22**, pp. 9-16.
9. Yang, Y. and Hughes, W. F., 1983, "An Elastohydrodynamic Analysis of Preloaded Sliding Seals," ASLE Transactions, **27**, pp. 197-202.
10. Prati, E. and Strozzi, A., 1984 "A Study of the Elastohydrodynamic Problem in Rectangular Elastomeric Seals," J. of Tribology, **24**, pp. 505-512.
11. Müller, H. K. and Nau, B. S., 1998, *Fluid Sealing Technology*, Marcel Dekker, New York.
12. Hirano, F. and Kaneta, M., 1971, "Theoretical Investigation of Friction and Sealing Characteristics of Flexible Seals for Reciprocating Motion," *Proc. 5th BHRA International Conference on Fluid Sealing*, G2.
13. Kanters, A. F. C., Verest, J. F. M. And Visscher, M., 1990, "On Reciprocating Elastomeric Seals: Calculation of Film Thicknesses Using the Inverse Hydrodynamic Lubrication Theory," Tribology Transactions, **33**, pp. 301-306.
14. Field, G. J., and Nau, B. S., 1973 "Film Thickness and Friction Measurements During Reciprocation of a Rectangular Section Rubber Seal Ring," *Proc. 6th BHRA International Conference on Fluid Sealing*, C5.
15. Kawahara, Y., Ohtake, Y. and Hirabayashi, H., 1981, "Oil Film Formation of Oil Seals for Reciprocating Motion," *Proc. 9th BHRA International Conference on Fluid Sealing*, C2.

16. Kanters, A. F. C. and Visscher, M., 1988, "Lubrication of Reciprocating Seals: Experiments on the Influence of Surface Roughness on Friction and Leakage," *Proc. 15th Leeds-Lyon Symposium on Tribology*, pp. 69-77.
17. Nikas, G. K., 2003, "Elastohydrodynamics and Mechanics of Rectangular Elastomeric Seals for Reciprocating Piston Rods," J. of Tribology, **125**, pp. 60-69.
18. Nikas, G. K, 2003, "Transient Elastohydrodynamic Lubrication of Rectangular Elastomeric Seals for Linear Hydraulic Actuators," J. of Engineering Tribology, **217**, pp. 461-473.
19. Nikas, G. K. and Sayles, R. S., 2004, "Nonlinear Elasticity of Rectangular Elastomeric Seals and its Effect on Elastohydrodynamic Numerical Analysis," Tribology International, **37**, pp. 651-660.
20. Patir, N. and Cheng, H. S., 1978, "An Average Flow Model for Determining Effects of Three-Dimensional Roughness on Partial Hydrodynamic Lubrication," J. of Lubrication Technology, **100**, pp. 12-17.
21. Patir, N. and Cheng, H. S., 1979, "Application of Average Flow Model to Lubrication Between Rough Sliding Surfaces," J. of Lubrication Technology, **101**, pp. 220-229.
22. Greenwood, J. A. and Williamson, J. B. P., 1966, "Contact of Nominally Flat Rough Surfaces," Proc. Royal Society (London), **A295**, pp. 300-319.
23. Streator, J. L., 2001, "A Model of Mixed Lubrication with Capillary Effects," *Proc. 15th Leeds-Lyon Symposium on Tribology*, pp. 121-128.
24. Salant, R. F., Maser, N. and Yang, B., 2006, "Elastohydrodynamic Model of a Reciprocating Hydraulic Rod Seal," AITC-AIT 5th International Conference on Tribology, Parma, Italy.
25. Salant, R. F., Maser, N. and Yang, B., 2006, "Numerical Model of a Reciprocating Hydraulic Rod Seal, Including Seal Roughness and Mixed Lubrication," 14th International Sealing Conference, Stuttgart, Germany.
26. Salant, R. F., Maser, N. and Yang, B., 2007, "Numerical Model of a Reciprocating Hydraulic Rod Seal," Journal of Tribology, **129**, pp. 91-97.